Line intensities of 12C2H2 in the 1.3, 1.2, and 1 μm spectral regions

David Jacquemart, Nelly Lacome, Jean-Yves Mandin

Line intensities of $^{12}C_2H_2$ in the 1.3, 1.2, and 1 μm spectral regions

D. Jacquemart [a,b,*], N. Lacome [a,b], J.-Y. Mandin [c,d]

[a] *UPMC Univ Paris 06, UMR 7075, Laboratoire de Dynamique Interactions et Réactivité, Case courrier 49, Bât. F 74, 4, place Jussieu, 75252 Paris Cedex 05, France*

[b] *CNRS, UMR 7075, Laboratoire de Dynamique Interactions et Réactivité, Case courrier 49, Bât. F 74, 4, place Jussieu, 75252 Paris Cedex 05, France*

[c] *UPMC Univ Paris 06, UMR 7092, Laboratoire de Physique Moléculaire pour l'Atmosphère et l'Astrophysique, Case courrier 76, 4, place Jussieu, 75252 Paris Cedex 05, France*

[d] *CNRS, UMR 7092, Laboratoire de Physique Moléculaire pour l'Atmosphère et l'Astrophysique, Case courrier 76, 4, place Jussieu, 75252 Paris Cedex 05, France*

Received 2008

* Corresponding author. Tel.: + 33-1-44-27-36-82; fax: + 33-1-44-27-30-21.
E-mail address: jacquemart@spmol.jussieu.fr (D. Jacquemart).

Abstract

Intensities of about 320 lines of the $^{12}C_2H_2$ molecule, belonging to 7 parallel bands, are measured in the 1.3, 1.2, and 1 μm spectral regions, with a mean accuracy around 3 or 7% depending on the spectral region. Vibrational transition dipole moment squared values and Herman-Wallis coefficients are obtained for each band, in order to model the rotational dependence of the transition dipole moment squared, except for the $\nu_1 + \nu_3 + 2\nu_4^0$ band at 7732.78 cm^{-1} that exhibits an unusual rotational dependence because of a strong ℓ-type resonance. HITRAN format line lists are set up for applications.

Keywords: Acetylene; Infrared; Vibro-rotational transitions; Line parameters; Databases

1. Introduction

The near infrared spectral range being very important in the field of optical communications, $^{12}C_2H_2$ was one of the molecules chosen to furnish wavenumber reference standards in this range. Mainly in this aim, Vander Auwera et al [1] published absolute wavenumbers of acetylene lines in the 1.4, 1.3, 1.2, and 1 µm spectral regions. In a previous work [2], we measured acetylene line intensities in the 1.4 µm region. The present paper report the results of line intensity measurements in the three remaining regions of interest, namely around 1.3, 1.2, and 1 µm.

First of all, let us recall the notations used throughout this paper. According to [3] and [4], we will note P the pseudo-quantum number equal to $5v_1 + 3v_2 + 5v_3 + v_4 + v_5$, where v_1, v_2, v_3, v_4, and v_5 are the quantum numbers associated with the normal modes of vibration of the molecule. A given value of P is assigned to a given set of interacting vibrational states, named polyad or cluster, polyads being also noted $\{Pv_5\}$. To label the vibrational levels, we will use the notations of Plíva [5,6]: vibrational levels will be noted $v_1\ v_2\ v_3\ (v_4\ v_5)^{\ell}_{\pm}\ r$, with $\ell = |\ell_4 + \ell_5|$, ℓ_t being the vibrational angular momentum quantum number associated with the degenerated bending mode t, ± being the symmetry type for Σ vibrational states ($\ell = 0$), and r a roman numeral indicating the rank of the level, by decreasing energy value (r = I for the highest energy level), inside the set of states having the same vibrational symmetry, and coupled by ℓ-type resonances. With these notations, the vibrational states and bands involved in this work are listed in Table 1. They concern the sequences of vibrational transitions ΔP = 12, 13, and 15, corresponding to the 1.3, 1.2, and 1 µm spectral regions, respectively. It is 6 cold bands of the $\Sigma^+_u \leftarrow \Sigma^+_g$ type, and one hot band of the $\Pi_u \leftarrow \Pi_g$ type.

An exhaustive bibliography being given in [1], we will recall here only some references useful for our purpose. As far as line position measurements and spectroscopic analysis are concerned, one should refer mainly to [1,7-15]. For intensity data, one can refer to the following works. Around 1.3 µm, Moriwaki et al [9] gave intensity measured values for five P lines of two bands. Around 1.2 µm, Kou et

al [11] gave relative observed and calculated values for the vibrational transition dipole moment squared of four bands. Similar data were given again in [15] by Abbouti Temsamani et al. Around 1 µm, Smith and Winn [8] gave relative observed intensity data for three bands. Herman et al [10] gave the results of measurements and calculations for the vibrational transition dipole moment squared of three bands. Some observed and calculated similar values were also given in [15] for more bands. All these works show that intensity data are very scarse, and that most of them are relative band intensity values or similar data of average accuracy. In the following, we will rely on the results of Abbouti Temsamani [16] who gave values of vibrational transition dipole moments squared for five of the bands we studied around 1.2 and 1 µm. This author estimated the precision and the accuracy of his results to be 5% and 15% respectively, due to the uncertainties on the temperature and mainly on the pressure measurements. Though intensities of individual lines are not reported in [16], those results will be useful for us for comparison purpose.

Using Fourier transform spectra, we have measured absolute intensities for 319 lines belonging to 7 bands around 1.3, 1.2, and 1 µm. Their mean accuracy is about 3 and 7% depending on the spectral region. Section 2 of the paper will be devoted to the experimental conditions and to the measurements. The results will also be given in this section. In Section 3, the data reduction and the calculation of line lists for applications will be discussed.

2. Line intensity measurements

2.1. Experimental details

To study C_2H_2 between 7600 and 9900 cm^{-1}, 9 spectra have been obtained with the rapid scan Bruker IFS 120 HR interferometer of LADIR (Paris). Experimental conditions are gathered in Table 2. These spectra were already used to study C_2H_2 around 1.4 µm [2], together with other spectra recorded at GSMA (Reims). Let us recall that the Bruker was equipped with a Globar source, CaF_2 beam splitter, an

InSb detector, and an optical filter (500-12500 cm^{-1}). The whole optical path was under vacuum and a multipass cell of 1-m base length was used. The cell was equipped with KCl windows. The temperature of the gas in the cell was recorded via four platinum probes at different places inside the cell. The uncertainty on the temperature measurements has been estimated to be ±0.5 K. The pressure of the gas was measured with a capacitive MKS Baratron manometer with an accuracy estimated to be about ±0.5%. Each scan among at least 390 recorded for every spectrum has then been individually transformed to a spectrum using the Fourier transform procedure included in the Bruker software OPUS package [17], selecting a Mertz phase error correction [18,19]. In the spectral regions studied in the present work, the SNR is not so good than around 1.4 μm, and it decreases towards high wavenumbers, leading to less accurate line intensities (see Table 1).

2.2. Method of measurement and results

To derive line intensities from the spectra, a multispectrum fitting (MSF) procedure [20] was used in the following conditions. As in [2], the absorption coefficient of the lines was calculated as a Voigt profile. The self-broadening coefficients were fixed at the values calculated according to [21], and the self-shifting coefficients were fixed at zero. Finally, 319 line intensities could be obtained. More than 20 of them are additional lines vs [1], they correspond to high *J* values. Lines are listed in Tables 3 and 4 for two bands that we will discuss in Section 3.1. The whole list of results is available as supplementary material to the paper.

To estimate the accuracy of our results, let us recall the cross comparisons performed in previous works [2,22]. First, line intensities measured in the 6600 cm^{-1} spectral region from the GSMA spectra [21] were found in very good agreement with those of El Hachtouki and Vander Auwera [23], i.e., (0.20 ± 0.64)%, with 1 SD after the ± sign. In the same way, the average difference found between line intensities measured separately in the GSMA and LADIR spectra, around 7500 cm^{-1}, is

(0.74 ± 1.30)% [2]. Considering this very good consistency, the whole accuracy of line intensities could therefore be expected very good too. The accuracy of intensities reported in this paper for well isolated lines is estimated to be about 3% around 1.3 and 1.2 µm, but only about 7% around 1 µm because of the decrease of the SNR with increasing wavenumber (see Tables 1 and 2). For very weak lines, the uncertainty can reach 10% or more.

The aim of this work was not to measure accurate line positions, already obtained in [1]. However, it is interesting to perform comparisons. The average difference between our measured line positions and those of [1] is $(-0.027 \pm 0.130) \times 10^{-3}$ cm^{-1}, with a mean of the 2 SD confidence intervals of our fits equal to 2×10^{-5} cm^{-1}. This is a very acceptable agreement compared with the absolute uncertainty of 2×10^{-4} cm^{-1} announced in [1], that is probably better. However, the difference between our line positions and those of [1] goes roughly from $+0.03 \times 10^{-3}$ cm^{-1} to -0.2×10^{-3} cm^{-1}, for the wavenumber from 7700 to 9800 cm^{-1}. Again, this is due to the increasing noise towards the end of our spectra.

3. Data reduction and calculation of line lists for applications

3.1. Data reduction

From a line intensity $S(T_0)$ derived from the multispectrum fitting procedure, expressed in cm·molecule^{-1} at the standard temperature T_0 = 296 K for pure $^{12}C_2H_2$, i.e., for a sample containing 100% of $^{12}C_2H_2$, we used the following formula to deduce the transition dipole moment squared $|R|^2$, in D^2 (1 debye = 3.33546×10^{-30} C·m)

$$S(T_0) = (1/4\pi\varepsilon_0)\,(8\pi^3/3hc)\,[g''\nu_0/g_V Q(T_0)]\,|R|^2\,L(J,\ell)\,\exp(-hcE''/kT_0)\,[1-\exp(-hc\nu_0/kT_0)], \qquad (1)$$

where $1/4\pi\varepsilon_0 = 10^{-36}$ erg·cm^3·D^{-2}; h is Planck's constant equal to $6.6260755 \times 10^{-27}$ erg·s (1 erg = 10^{-7} J); c is vacuum speed of light equal to $2.99792458 \times 10^{10}$ cm·s^{-1}; g'' is the statistical weight due to nuclear spin of the lower level (1 for *s*-type levels and 3 for *a*-type levels); ν_0 is the transition wavenumber in cm^{-1}; g_V depends on the degeneracy of the levels involved, being 2 if both upper and lower vibrational states are degenerated and 1 otherwise; $Q(T_0)$ is the total internal partition function at temperature T_0; $L(J,\ell)$ is the Hönl-London factor, J being the rotational quantum number of the lower level of the transition, and ℓ its secondary vibrational quantum number ($\ell = |\ell_4 + \ell_5|$); E'' , in cm^{-1}, is the energy of the lower level; k is Boltzmann's constant equal to 1.380658×10^{-16} erg·K^{-1}. For parallel bands studied in this work ($\Delta\ell = 0$), the Hönl-London factors are given by

$$L(J,\ell) = (J+1+\ell)\,(J+1-\ell) / (J+1) \quad (R\text{-branch}), \tag{2}$$

$$L(J,\ell) = (J+\ell)\,(J-\ell) / J \quad (P\text{-branch}). \tag{3}$$

In Eq. (1), the E'' energy values have been taken from the HITRAN database [24]. To calculate the partition function $Q(T_0)$, we used the values tabulated by Fischer et al [25]. At 296 K, $Q(T_0)$ is equal to 414.03.

Data reduction was achieved by fitting the measured transition dipole moments squared to the following effective expression

$$|R|^2 = |R_0|^2\,(1 + A_1\ m + A_2\ m^2)^2. \tag{4}$$

m is equal to $-J$ in the *P*-branch and J+1 in the *R*-branch. $|R_0|^2$ is the vibrational transition dipole moment squared, and A_1 and A_2 are Herman-Wallis coefficients. Transition dipole moment squared values, $|R|^2$, deduced from the experimental line intensities are reported in Tables 3 and 4 for two selected bands. The

whole list of experimental values of $|R|^2$ is included in the supplementary material. Vibrational transition dipole moment squared values, $|R_0|^2$, and Herman-Wallis coefficients obtained from an unweighted fit of the $|R|^2$'s, are listed in Table 5. The $|R_0|^2$ values obtained for bands around 8500 and 9600 cm^{-1} by Abbouti Temsamani [16] are also quoted for comparison. Having in mind the 15% accuracy announced in [16], the agreement is good (4% on the average).

In the *P* branch of the $3\nu_3 + \nu_4^1 - \nu_4^1$ band, the *e* and *f* components are unresolved for several values of *J*, and consequently could not be measured. For this band, the two *e* and *f* sub-branches were adjusted simultaneously, leading to the same value of $|R_0|^2$. The rotational dependence of $|R|^2$ for the studied bands can easily be modelled by the usual Herman-Wallis factor. The case of the $\nu_1 + 2\nu_2 + (\nu_4 + \nu_5)^0_+$ band is a typical example (see Fig. 1). Figure 2 shows the particular case of the $\nu_1 + \nu_2 + \nu_3$ band, for which $|R|^2$ does not exhibit any significant rotational dependence (see Table 4), that is exceptional for *P* and *R* branches of the acetylene molecule. The case of the $\nu_1 + \nu_3 + 2\nu_4^0$ band is more surprising (see Fig. 3). Except for very few lines, for which $|R|^2$ departs slightly (less than about 3%) from the general tendency of other values, $|R|^2$ shows a very regular variation vs *m*. However, it cannot be fitted by a polynomial curve. Such a rotational dependence, that had never been observed before for C_2H_2, is probably due to the ℓ-type resonance existing between the levels $101(20)^0_+$ and $101(20)^2e$, very close to each other (about 4 cm^{-1}). As pointed out by Moriwaki et al [9], this strong interaction makes the forbidden $\Delta \leftarrow \Sigma$ band $\nu_1 + \nu_3 + 2\nu_4^2$ observable around 7737 cm^{-1}. Unfortunately, this band is too weak in our spectra to allow reliable intensity measurements.

3.2. Line lists for databases

As spectroscopic databases do not contain any data for acetylene in the involved spectral regions, the next step of this work is to generate line lists for applications, by adding intensity information to existing wavenumbers. To set up HITRAN format line lists, the absolute line wavenumbers measured by

Vander Auwera et al have been taken from [1] with an uncertainty code 4 (accuracy between 10^{-4} and 10^{-3} cm^{-1}). Lines flagged by an asterisk in [1] have received a code 3 (accuracy between 10^{-3} and 10^{-2} cm^{-1}). A few lines missing in [1], as well as some additional lines that could be measured in our spectra, had their position calculated through an empirical polynomial fit based on measured values. Those lines have received a code 3. Line intensities have been calculated using the constants of Table 5. Uncertainty codes for line intensities have been chosen according to the accuracies quoted in Table 1, namely code 6 (uncertainty between 2 and 5%) for bands at 1.3 and 1.2 µm, and code 5 (uncertainty between 5 and 10%) for bands at 1 µm. Extrapolated line intensities have received a code 5. For the $\nu_1 + \nu_3 + 2\nu_4^0$ band, the experimental $|R|^2$ values cannot be fitted by the Herman-Wallis factor. In the line list, line intensities calculated for this band have been obtained from experimental $|R|^2$ values, except for missing lines, and for a few measured ones, for which more precise smoothed calculated values of $|R|^2$ have been obtained from a linear interpolation between the values of neigbooring lines. Note that in the HITRAN format line lists, $|R|^2$ values have been put in place of the Einstein-*A* coefficients, and that the statistical weights have not been reported.

These line lists contain 484 lines and will be proposed to the HITRAN [24] and GEISA [26] databases. They are also included in the supplementary material. Table 6 summarizes the data now available for the $^{12}C_2H_2$ molecule in the studied spectral regions. To facilitate comparisons, this table has been set up in the same format as in [2]. The first part gives a synthetic view, whereas the second part gives more details concerning each band in the involved spectral regions.

4. Conclusion

The three spectral regions around 1.3, 1.2, and 1 µm of the acetylene molecule being of metrological interest, absolute line wavenumbers were published few years ago for 7 bands [1], but systematic and absolute measurements of line intensities had never been performed for these bands. The

aim of this work was to acquire line intensity data in these spectral domains of C_2H_2, in order to enrich spectroscopic databases. These spectral domains also have a theoretical interest. Thus, when reducing the data, an anomalous rotational dependance was observed for the transition dipole moment squared of the $\nu_1 + \nu_3 + 2\nu_4^0$ band, because of a strong ℓ-type resonance. To perform a more detailed analysis, it will be necessary to obtain spectra where many more interacting bands, as also hot bands, would be observed.

Acknowledgements

Pr. V. Dana is acknowledged for useful discussions and a careful reading of the manuscript.

References

[1] Vander Auwera J, El Hachtouki R, Brown LR. Absolute line wavenumbers in the near infrared: $^{12}C_2H_2$ and $^{12}C^{16}O_2$. Mol Phys 2002;100:3563-76.

[2] Jacquemart D, Lacome N, Mandin JY, Dana V, Tran H, Gueye K, Lyulin OM, Perevalov VI, Régalia-Jarlot L. The IR spectrum of $^{12}C_2H_2$: line intensity measurements in the 1.4 μm region and update of the databases. JQSRT, accepted for publication.

[3] Kelman ME, Gengxin C. Approximate constants of motion and energy transfer pathways in highly excited acetylene. J Chem Phys 1991;95:8671-2.

[4] Perevalov VI, Lobodenko EI, Teffo JL. Reduced effective Hamiltonian for global fitting of C_2H_2 rovibrational lines. In: Proceedings of the XIIth Symposium and school on high-resolution molecular spectroscopy. St. Petersburg, Russian Federation. SPIE 1997;3090:143-9.

[5] Plíva J. Spectrum of acetylene in the 5-micron region. J Mol Spectrosc 1972;44:145-64.

[6] Plíva J. Molecular constants for the bending modes of acetylene $^{12}C_2H_2$. J Mol Spectrosc 1972;44:165-82.

[7] Ghersetti S, Adams JE, Rao KN. $^{12}C_2H_2$ and $^{12}C_2HD$ bands at 1.1 μm. J Molec Spectrosc 1977;64:157-61.

[8] Smith BC, Winn JS. The C–H overtone spectra of acetylene: bend/stretch interactions below 10000 cm^{-1}. J Chem Phys 1988;89:4638-45.

[9] Moriwaki N, Tsuchida T, Takehisa Y, Ohashi N. 1.3 μm DFB diode laser spectroscopy of $^{12}C_2H_2$. J Mol Spectrosc 1989;137:230-4.

[10] Herman M, Huet TR, Vervloet M. Spectroscopy and vibrational couplings in the $3\nu_3$ region of acetylene. Mol Pys 1989;66:333-53.

[11] Kou Q, Guelachvili G, Abbouti Temsamani M, Herman M. The absorption spectrum of C_2H_2 around $\nu_1+\nu_3$: energy standards in the 1.5 μm region and vibrational clustering. Can J Phys 1994;72:1241-50.

[12] Abbouti Temsamani M, Herman M. The vibrational energy pattern in $^{12}C_2H_2$ (II): vibrational clustering and rotational structure. J Chem Phys 1996;105:1355-62.

[13] El Idrissi MI, Liévin J, Campargue A, Herman M. The vibrational energy pattern in acetylene (IV): updated global vibration constants for $^{12}C_2H_2$. J Chem Phys 1999;110:2074-86.

[14] Campargue A, Bertseva E, Ding Y. The overtone spectrum of C_2D_2 and C_2H_2 by ICLAS-VECSEL near 1 μm. J Mol Spectrosc 2003;220:13-8.

[15] Abbouti Temsamani M, Champion JM, Oss S. Infrared transition intensities in acetylene : an algebraic approach. J Chem Phys 1999;110 :2893-902.

[16] Abbouti Temsamani M. Acetylene $X\ ^1\Sigma^+_g$: from high resolution to intramolecular dynamics. Thesis. Université Libre de Bruxelles. Belgium; 1996.

[17] Wartewig S. IR and Raman Spectroscopy: Fundamental Processing. Weinheim: Wiley-VCH; 2003.

[18] Mertz L. Transformations in Optics. New York: Wiley; 1965.

[19] Griffiths PR, deHaseth JA. Fourier Transform Infrared Spectrometry. New York: Wiley; 1986.

[20] Jacquemart D, Mandin JY, Dana V, Picqué N, Guelachvili G. A multispectrum fitting procedure to deduce molecular line parameters. Application to the 3–0 band of $^{12}C^{16}O$. Eur Phys J D 2001;14:55-69.

[21] Jacquemart D, Mandin JY, Dana V, Régalia-Jarlot L, Plateaux JJ, Décatoire D, Rothman LS. The spectrum of acetylene in the 5-μm region from new line-parameter measurements. JQSRT 2003;76:237-67.

[22] Tran H, Mandin JY, Dana V, Régalia-Jarlot L, Thomas X, Von der Heyden P. Line intensities in the 1.5-μm spectral region of acetylene. JQSRT 2007;108:342-62.

[23] El Hachtouki R, Vander Auwera J. Absolute line intensities in acetylene: the 1.5 μm region. J Mol Spectrosc 2002;216:355-62.

[24] Rothman LS, Jacquemart D, Barbe A, Benner DC, et al. The Hitran 2004 Molecular Spectroscopic Database. JQSRT 2005;96:139-204.

[25] Fischer J, Gamache RR, Goldman A, Rothman LS, Perrin A. Total internal partition sums for molecular species in the 2000 edition of the HITRAN database. JQSRT 2003;82:401-12.

[26] Jacquinet-Husson N, Scott NA, Chédin A, Garceran K, et al. The 2003 edition of GEISA / IASI spectroscopic database. JQSRT 2005;95:429-67.

Captions of tables

Table 1

List of the bands observed in the ΔP = 12, 13, and 15 series of transitions of $^{12}C_2H_2$ between 7600 and 9900 cm^{-1}

Table 2

Experimental conditions and characteristics of the spectra recorded in Paris (LADIR)

Table 3

Line positions and intensities for the $\nu_1 + \nu_3 + 2\nu_4{}^0$ band of $^{12}C_2H_2$ at 7732.78 cm^{-1}

Table 4

Line positions and intensities for the $\nu_1 + \nu_2 + \nu_3$ band of $^{12}C_2H_2$ at 8512.06 cm^{-1}

Table 5

Summary of $^{12}C_2H_2$ experimental vibrational transition dipole moments squared $|R_0|^2$ in D^2 (1 D = 3.33546 × 10^{-30} C·m), and Herman-Wallis coefficients, see Eq. (4), for bands observed between 7600 and 9900 cm^{-1} [a]. Comparison with previous results

Table 6

Summary of new bands and transitions now available for the $^{12}C_2H_2$ molecule at 1.3, 1.2, and 1 μm

Captions of figures

Fig. 1. Variation of the transition dipole moment squared $|R|^2$, in D^2 (1 D = 3.33546 × 10^{-30} C·m), vs. *m*, for the $\nu_1 + 2\nu_2 + (\nu_4 + \nu_5)^0_+$ band at 8556.60 cm^{-1}. The solid line represents the values calculated using the constants reported in Table 5. For this band, the rotational dependence is typical of what is usually observed for C_2H_2, and is well described by the Herman-Wallis factor, see Eq. (4).

Fig. 2. Variation of the transition dipole moment squared $|R|^2$, in D^2 (1 D = 3.33546 × 10^{-30} C·m), vs. *m*, for the $\nu_1 + \nu_2 + \nu_3$ band at 8512.06 cm^{-1}. The horizontal line represents $|R_0|^2 = 5.21 \times 10^{-7}$ D^2 (see Tables 4 and 5). For this band, no rotational dependence is observed (the Herman-Wallis factor is equal to unity).

Fig. 3. Variation of the transition dipole moment squared $|R|^2$, in D^2 (1 D = 3.33546 × 10^{-30} C·m), vs. *m*, for the $\nu_1 + \nu_3 + 2\nu_4^0$ band at 7732.78 cm^{-1} (see Table 3). The Herman-Wallis factor is unadapted to fit such an unusual rotational dependence.

Table 1

List of the bands observed in the ΔP = 12, 13, and 15 series of transitions of $^{12}C_2H_2$ between 7600 and 9900 cm^{-1}

Band	Center [a]	Upper level [b]	Polyad [c]	Symmetry	N [d]	% [e]	PJ_{max}-RJ_{max} [f]
$\nu_1 + \nu_3 + 2\nu_4^0$	7732.78	$101(20)^0_+$	$\{12\nu_5\}$	$\Sigma^+_u \leftarrow \Sigma^+_g$	38	3 %	23-21
$\nu_1 + \nu_2 + \nu_3$	8512.06	$111(00)^0_+$	$\{13\nu_5\}$	$\Sigma^+_u \leftarrow \Sigma^+_g$	58	3 %	31-30
$\nu_1 + 2\nu_2 + (\nu_4 + \nu_5)^0_+$	8556.60	$120(11)^0_+$	$\{13\nu_5\}$	$\Sigma^+_u \leftarrow \Sigma^+_g$	33	3 %	25-25
$3\nu_3$	9639.87	$003(00)^0_+$	$\{15\nu_5\}$	$\Sigma^+_u \leftarrow \Sigma^+_g$	61	7 %	33-33
$\nu_1 + \nu_2 + \nu_3 + 2\nu_4^0$	9668.17	$111(20)^0_+$	$\{15\nu_5\}$	$\Sigma^+_u \leftarrow \Sigma^+_g$	33	7 %	25-25
$2\nu_1 + \nu_3$	9835.18	$201(00)^0_+$	$\{15\nu_5\}$	$\Sigma^+_u \leftarrow \Sigma^+_g$	54	7 %	29-29
$3\nu_3 + \nu_4^1 - \nu_4^1$	9602.66	$003(10)^1$	$\{16\nu_5\}$	$\Pi_u \leftarrow \Pi_g$	42	7 %	26-18

[a] Rough values of band centers, in cm^{-1}, compiled from [1].

[b] Upper vibrational level.

[c] Polyad from which the upper vibrational level belongs.

[d] Number of line intensities measured in each band.

[e] Estimated mean accuracy of measured line intensities.

[f] Maximum J values of the lines whose intensity could be measured, in P and R branches.

Table 2

Experimental conditions and characteristics of the spectra recorded in Paris (LADIR)

Commercial sample (Air Liquide Alphagaz)	
Natural C_2H_2	97.760% of $^{12}C_2H_2$
Stated purity	99.55%
Maximum path difference	90 cm
Unapodized FWHM resolution	$\approx 5.6 \times 10^{-3}$ cm^{-1}
Spectral step after post-zero filling	3.77×10^{-3} cm^{-1}
SNR around 7200 cm^{-1}	≈ 1000
around 7700 cm^{-1}	≈ 200
around 8500 cm^{-1}	≈ 100
around 9600 cm^{-1}	≈ 50
Collimator focal length	418 mm
Nominal iris radius	0.40 mm
Effective iris radius	0.45(1) mm [a]
Free spectral range	5500-11000 cm^{-1}
Involved spectral domain	7600-9900 cm^{-1}

Spectrum Number [b]	Total pressure ±0.5% [c] (hPa)	Absorbing path ±1 cm [c]	Temperature ±0.5 K [c]
16	3.224	2015	296.95
17	8.316	2015	296.95
18	9.361	2015	296.00
19	16.56	2015	296.95
20	20.72	2015	296.00
21	26.43	2015	296.95
22	46.03	2015	298.15
23	53.20	2015	296.00
24	92.20	2015	296.00

[a] 1 SD between parentheses in unit of the last digit.

[b] Same spectra as in [2].

[c] Absolute uncertainty (excess digits are given as a guide).

Table 3

Line positions and intensities for the $\nu_1 + \nu_3 + 2\nu_4^0$ band of $^{12}C_2H_2$ at 7732.78 cm^{-1}

Line	This work [a]	[1] [b]	Dif [c]	S_{obs} [d]	$\|R\|^2_{obs}$ [e]
Pee23	7676.44907	7676.44806	1.01	6.754E-25	2.973E-08
Pee21	7681.49754	7681.49718	0.36	1.049E-24	3.022E-08
Pee20	7684.01024	7684.00937	0.87	4.200E-25	2.998E-08
Pee19	7686.51523	7686.51540	-0.17	1.506E-24	3.001E-08
Pee17	7691.50220	7691.50207	0.13	2.104E-24	3.068E-08
Pee15	7696.45763	7696.45758	0.05	2.786E-24	3.156E-08
Pee14	7698.92912	7698.92942	-0.30	1.052E-24	3.224E-08
Pee13	7701.38861	7701.38885	-0.24	3.580E-24	3.356E-08
Pee12	7703.84020	7703.84035	-0.15	1.300E-24	3.413E-08
Pee11	7706.28812	7706.28835	-0.23	4.255E-24	3.540E-08
Pee10	7708.72879	7708.72870	0.09	1.510E-24	3.654E-08
Pee 9	7711.16434	7711.16463	-0.29	4.907E-24	3.921E-08
Pee 8	7713.59531	7713.59512	0.19	1.679E-24	4.085E-08
Pee 7	7716.02166	7716.02182	-0.16	5.258E-24	4.446E-08
Pee 6	7718.44466	7718.44513	-0.47	1.737E-24	4.742E-08
Pee 5	7720.86369	7720.86395	-0.26	4.821E-24	4.915E-08
Pee 4	7723.27640	7723.27612	0.28	1.410E-24	5.089E-08
Pee 3	7725.67911	7725.67931	-0.20	3.330E-24	5.101E-08
Pee 1	7730.44052	7730.44040	0.12	1.171E-24	5.078E-08
Ree 1	7737.44544	7737.44566	-0.22	2.320E-24	5.027E-08
Ree 2	7739.74870	7739.74772	0.98	1.102E-24	4.887E-08
Ree 3	7742.04230	7742.04218	0.12	4.179E-24	4.792E-08
Ree 4	7744.32876	7744.32909	-0.33	1.607E-24	4.626E-08
Ree 5	7746.61095	7746.61112	-0.17	5.128E-24	4.342E-08
Ree 6	7748.88891	7748.88939	-0.48	1.741E-24	4.059E-08
Ree 7	7751.16230	7751.16244	-0.14	5.166E-24	3.804E-08
Ree 8	7753.43011	7753.43032	-0.21	1.711E-24	3.680E-08
Ree 9	7755.69188	7755.69213	-0.25	4.785E-24	3.422E-08
Ree10	7757.94590	7757.94584	0.06	1.472E-24	3.218E-08
Ree11	7760.19534	7760.19545	-0.11	4.156E-24	3.147E-08
Ree12	7762.43629	7762.43594	0.35	1.290E-24	3.102E-08
Ree13	7764.66318	7764.66351	-0.33	3.395E-24	2.931E-08
Ree14	7766.88749	7766.88771	-0.22	1.020E-24	2.892E-08
Ree15	7769.10209	7769.10198	0.11	2.715E-24	2.856E-08
Ree16	7771.30733	7771.30667	0.66	7.988E-25	2.847E-08
Ree17	7773.50381	7773.50408	-0.27	2.042E-24	2.782E-08
Ree18	7775.69141	7775.69046	0.95	5.732E-25	2.726E-08
Ree21	7782.19824	7782.19831	-0.07	9.842E-25	2.672E-08

[a] Line position measured in this work, in cm^{-1}.

[b] Standard line position measured by Vander Auwera et al [1].

[c] Difference between line position measured in this work and the standard value of [1], in 10^{-3} cm^{-1}.

[d] Measured line intensity, for pure $^{12}C_2H_2$ (i.e., for a sample containing 100% of $^{12}C_2H_2$), in cm·molecule^{-1} at 296 K.

[e] Experimental transition dipole moment squared value, in D^2 (1 D = 3.33546×10^{-30} C·m), deduced from S_{obs}.

Table 4

Line positions and intensities for the $\nu_1 + \nu_2 + \nu_3$ band of $^{12}C_2H_2$ at 8512.06 cm^{-1}

Line	This work [a]	[1] [b]	Dif [c]	S_{obs} [d]	S_{calc} [d]	% [e]	$\|R\|^2_{obs}$ [f]
Pee31	8421.85411	8421.85349	0.62	1.431E-24	1.421E-24	0.69	5.246E-07
Pee29	8428.74010	8428.73991	0.19	2.739E-24	2.668E-24	2.60	5.349E-07
Pee27	8435.47984	8435.47970	0.14	4.907E-24	4.764E-24	2.91	5.366E-07
Pee26	8438.79453	8438.79547	-0.94	2.100E-24	2.082E-24	0.86	5.255E-07
Pee25	8442.07394	8442.07398	-0.04	8.224E-24	8.084E-24	1.70	5.300E-07
Pee23	8448.52106	8448.52128	-0.22	1.322E-23	1.302E-23	1.49	5.289E-07
Pee22	8451.68977	8451.69028	-0.51	5.506E-24	5.404E-24	1.86	5.309E-07
Pee21	8454.82205	8454.82241	-0.36	2.001E-23	1.990E-23	0.57	5.240E-07
Pee20	8457.91719	8457.91769	-0.50	8.143E-24	8.034E-24	1.34	5.281E-07
Pee19	8460.97582	8460.97611	-0.29	2.842E-23	2.879E-23	-1.30	5.143E-07
Pee18	8463.99667	8463.99703	-0.36	1.124E-23	1.130E-23	-0.56	5.181E-07
Pee17	8466.98249	8466.98283	-0.34	3.883E-23	3.934E-23	-1.32	5.142E-07
Pee16	8469.93050	8469.93083	-0.33	1.484E-23	1.499E-23	-1.01	5.158E-07
Pee15	8472.84169	8472.84197	-0.28	4.988E-23	5.065E-23	-1.54	5.131E-07
Pee14	8475.71586	8475.71610	-0.24	1.840E-23	1.871E-23	-1.70	5.123E-07
Pee13	8478.55316	8478.55335	-0.19	6.046E-23	6.119E-23	-1.20	5.148E-07
Pee12	8481.35330	8481.35359	-0.29	2.163E-23	2.185E-23	-1.01	5.158E-07
Pee11	8484.11655	8484.11669	-0.14	6.779E-23	6.896E-23	-1.72	5.122E-07
Pee10	8486.84273	8486.84287	-0.14	2.371E-23	2.370E-23	0.04	5.212E-07
Pee 9	8489.53172	8489.53172	0.00	7.114E-23	7.177E-23	-0.89	5.164E-07
Pee 8	8492.18330	8492.18357	-0.27	2.351E-23	2.358E-23	-0.31	5.194E-07
Pee 7	8494.79811	8494.79816	-0.05	6.763E-23	6.784E-23	-0.31	5.194E-07
Pee 6	8497.37536	8497.37559	-0.23	2.109E-23	2.101E-23	0.40	5.231E-07
Pee 5	8499.91565	8499.91563	0.02	5.579E-23	5.626E-23	-0.85	5.166E-07
Pee 4	8502.41830	8502.41882	-0.52	1.614E-23	1.589E-23	1.57	5.293E-07
Pee 3	8504.88411	8504.88412	-0.01	3.744E-23	3.745E-23	-0.02	5.209E-07
Pee 2	8507.31207	8507.31253	-0.46	8.670E-24	8.614E-24	0.65	5.244E-07
Pee 1	8509.70316	8509.70285	0.31	1.317E-23	1.322E-23	-0.37	5.191E-07
Ree 0	8514.37246	8514.37043	2.03	4.391E-24	4.460E-24	-1.58	5.129E-07
Ree 1	8516.65049	8516.65033	0.16	2.637E-23	2.647E-23	-0.39	5.190E-07
Ree 2	8518.89114	8518.89094	0.20	1.309E-23	1.294E-23	1.18	5.272E-07
Ree 3	8521.09430	8521.09415	0.15	4.977E-23	5.001E-23	-0.48	5.185E-07
Ree 4	8523.25975	8523.25955	0.20	2.025E-23	1.991E-23	1.68	5.299E-07
Ree 5	8525.38753	8525.38730	0.23	6.675E-23	6.772E-23	-1.46	5.135E-07
Ree 6	8527.47754	8527.47742	0.12	2.506E-23	2.459E-23	1.86	5.309E-07
Ree 7	8529.52984	8529.52969	0.15	7.609E-23	7.786E-23	-2.32	5.092E-07
Ree 8	8531.54431	8531.54417	0.14	2.743E-23	2.665E-23	2.83	5.362E-07
Ree 9	8533.52092	8533.52072	0.20	7.808E-23	8.017E-23	-2.68	5.074E-07
Ree10	8535.45961	8535.45942	0.19	2.651E-23	2.622E-23	1.08	5.267E-07
Ree11	8537.36039	8537.36016	0.23	7.423E-23	7.570E-23	-1.98	5.109E-07
Ree12	8539.22281	8539.22296	-0.15	2.379E-23	2.383E-23	-0.17	5.201E-07
Ree13	8541.04785	8541.04765	0.20	6.523E-23	6.639E-23	-1.78	5.119E-07
Ree14	8542.83414	8542.83430	-0.16	2.034E-23	2.020E-23	0.67	5.245E-07
Ree16	8546.29339	8546.29322	0.17	1.610E-23	1.608E-23	0.15	5.218E-07
Ree17	8547.96565	8547.96545	0.20	4.173E-23	4.205E-23	-0.77	5.170E-07
Ree18	8549.59951	8549.59930	0.21	1.209E-23	1.205E-23	0.36	5.229E-07
Ree19	8551.19520	8551.19510	0.10	3.039E-23	3.062E-23	-0.77	5.170E-07
Ree20	8552.75248	8552.75247	0.01	8.663E-24	8.530E-24	1.53	5.291E-07
Ree21	8554.27131	8554.27110	0.21	2.071E-23	2.110E-23	-1.86	5.115E-07
Ree22	8555.75224	8555.75202	0.22	5.758E-24	5.717E-24	0.71	5.247E-07

Table 4 (continued)

Line	This work [a]	[1] [b]	Dif [c]	S_{obs} [d]	S_{calc} [d]	% [e]	$\|R\|^2_{obs}$ [f]
Ree23	8557.19393	8557.19381	0.12	1.375E-23	1.377E-23	-0.13	5.203E-07
Ree24	8558.59746	8558.59736	0.10	3.679E-24	3.635E-24	1.19	5.273E-07
Ree25	8559.96243	8559.96232	0.11	8.560E-24	8.526E-24	0.40	5.231E-07
Ree26	8561.28803	8561.28822	-0.19	2.207E-24	2.194E-24	0.61	5.242E-07
Ree27	8562.57575	8562.57634	-0.59	5.067E-24	5.015E-24	1.03	5.264E-07
Ree28	8563.82498	8563.82672	-1.74	1.262E-24	1.258E-24	0.34	5.228E-07
Ree29	8565.03525	8565.03531	-0.06	2.798E-24	2.804E-24	-0.21	5.199E-07
Ree30	8566.20689	8566.20388	3.01	7.003E-25	6.861E-25	2.03	5.318E-07

[a] Line position measured in this work, in cm^{-1}.

[b] Standard line position measured by Vander Auwera et al [1].

[c] Difference between line position measured in this work and the standard value of [1], in 10^{-3} cm^{-1}.

[d] S_{obs} and S_{calc} are measured and calculated intensities, respectively, for pure $^{12}C_2H_2$ (i.e., for a sample containing 100% of $^{12}C_2H_2$), in cm·molecule^{-1} at 296 K.

[e] Ratio $100 \times (S_{obs} - S_{calc}) / S_{obs}$.

[f] Experimental transition dipole moment squared value, in D^2 (1 D = 3.33546×10^{-30} C·m), deduced from S_{obs}.

Table 5

Summary of $^{12}C_2H_2$ experimental vibrational transition dipole moments squared $|R_0|^2$ in D^2 (1 D = 3.33546×10^{-30} C·m), and Herman-Wallis coefficients, see Eq. (4), for bands observed between 7600 and 9900 cm^{-1} [a]. Comparison with previous results

Band	Center	$\|R_0\|^2$ in 10^{-7} D^2	$A_1 \times 10^{-4}$	$A_2 \times 10^{-4}$
$\nu_1 + \nu_3 + 2\nu_4^0$	7732.78	Herman-Wallis factor unadapted (see Table 3 and Fig. 3)		
$\nu_1 + \nu_2 + \nu_3$	8512.06	5.21(14) ± 0.16		
		5.28 ± 0.79 [b]		
$\nu_1 + 2\nu_2 + (\nu_4 + \nu_5)^0_+$	8556.60	0.2836(23) ± 0.0085	−3.1(19)	−1.13(14)
		0.257 ± 0.039 [b]		
$3\nu_3$	9639.87	16.72(19) ± 1.2		−0.23(11)
		19.7 ± 3.0 [b]		
$\nu_1 + \nu_2 + \nu_3 + 2\nu_4^0$	9668.17	1.673(17) ± 0.12	−8.6(26)	−4.33(18)
		1.13 ± 0.17 [b]		
$2\nu_1 + \nu_3$	9835.18	2.338(21) ± 0.16	+6.6(18)	−0.18(12)
		2.39 ± 0.36 [b]		
$3\nu_3 + \nu_4^1 - \nu_4^1$	9602.66	32.63(37) ± 2.3		

[a] 95% confidence intervals (2 SD, in unit of the last quoted digit) are given between parenthesis. For $|R_0|^2$ values, the overall accuracy (see Table 1) is reported after the ± sign. Non given Herman-Wallis coefficients have been fixed at zero.

[b] Results of Abbouti Temsamani [16]. Announced accuracy about 15%. Herman-Wallis coefficients were not determined in [16].

Table 6

Summary of new bands and transitions now available for the $^{12}C_2H_2$ molecule at 1.3, 1.2, and 1 μm

Spectral region (μm)	Number of bands [a] cold / hot	Number of transitions [a] cold / hot	Spectral domain (cm^{-1})	Intensity range ($cm \cdot molecule^{-1}$ at 296 K)
1.3	1 / 0	51 / 0	7671 - 7791	10^{-25} - 10^{-24}
1.2	2 / 0	132 / 0	8407 - 8612	10^{-26} - 10^{-22}
1.0	3 / 1	193 / 108	9516 - 9890	10^{-25} - 10^{-22}

Band [b]	Origin [b]	ν_{min} - ν_{max} [b]	ΣS [b]	S_{min} - S_{max} [b]	$J_{max}\nu/J_{max}S/J_{max}$ [b]			Cdν [b]	CdS [b]
1.3 μm spectral region									
101200+_–000000+	7732.78	7671-7791	9.5E-23	1.7E-25-5.1E-24	25-25	23-21	25-25	4/3	6/5
1.2 μm spectral region									
111000+_–000000+	8512.06	8407-8572	1.5E-21	1.6E-25-7.8E-23	33-33	31-30	35-35	4/3	6/5
120110+_–000000+	8556.60	8471-8613	8.0E-23	3.1E-26-4.1E-24	25-25	25-25	30-30	4/3	6/5
1.0 μm spectral region									
003101__–000101	9602.66	9516-9652	5.3E-22	1.2E-25-1.4E-23	26-20	26-18	30-25	4/3	5/5
003000+_–000000+	9639.87	9535-9700	5.5E-21	5.7E-25-2.8E-22	33-33	33-33	35-35	4/3	5/5
111200+_–000000+	9668.17	9587-9730	4.8E-22	1.1E-25-2.6E-23	25-25	25-25	30-30	4/3	5/5
201000+_–000000+	9835.18	9748-9890	7.8E-22	3.1E-25-4.1E-23	29-29	29-29	30-30	4/3	5/5

[a] HITRAN 2004 and GEISA 2003 do not contain data for the acetylene molecule in these spectral regions.

[b] Explanation of the column headings:

Band: vibrational assignment used in the line lists, according to Section 1: $v_1\ v_2\ v_3\ v_4\ v_5\ \ell \pm r$ for the upper and lower states. When ± or *r* does not occur for the upper state, it is replaced by an underscore (this is the case for the involved bands).

Origin: approximate value of the band center, in cm^{-1}.

ν_{min} - ν_{max} : limiting values of line positions, in cm^{-1}.

ΣS : sum of line intensities, in cm·molecule^{-1} at 296 K.

S_{min} - S_{max} : limiting values of line intensities, in cm·molecule^{-1} at 296 K.

$J_{max}\nu$: maximum value of J for which a line position has been measured.

$J_{max}S$: maximum value of J for which a line intensity has been measured.

J_{max} : maximum value of J present in the line list.

(The first value is for the *P*-branch and the second for the *R*-branch.)

Cdν: uncertainty code for line positions [24]. Code 3: 10^{-3}-10^{-2} cm^{-1}. Code 4: 10^{-4}-10^{-3} cm^{-1}.

Cd*S*: uncertainty code for line intensities [24]. Code 5: 5-10%. Code 6: 2-5%.

(The second value is for interpolated or extrapolated lines.)

Other spectroscopic data are the same as those already put in the last updates of the databases: air- and self-broadening coefficients, default value for the temperature exponent of air-broadening coefficients, constant value for the air-pressure shifting coefficient, and their accuracies [2,24].

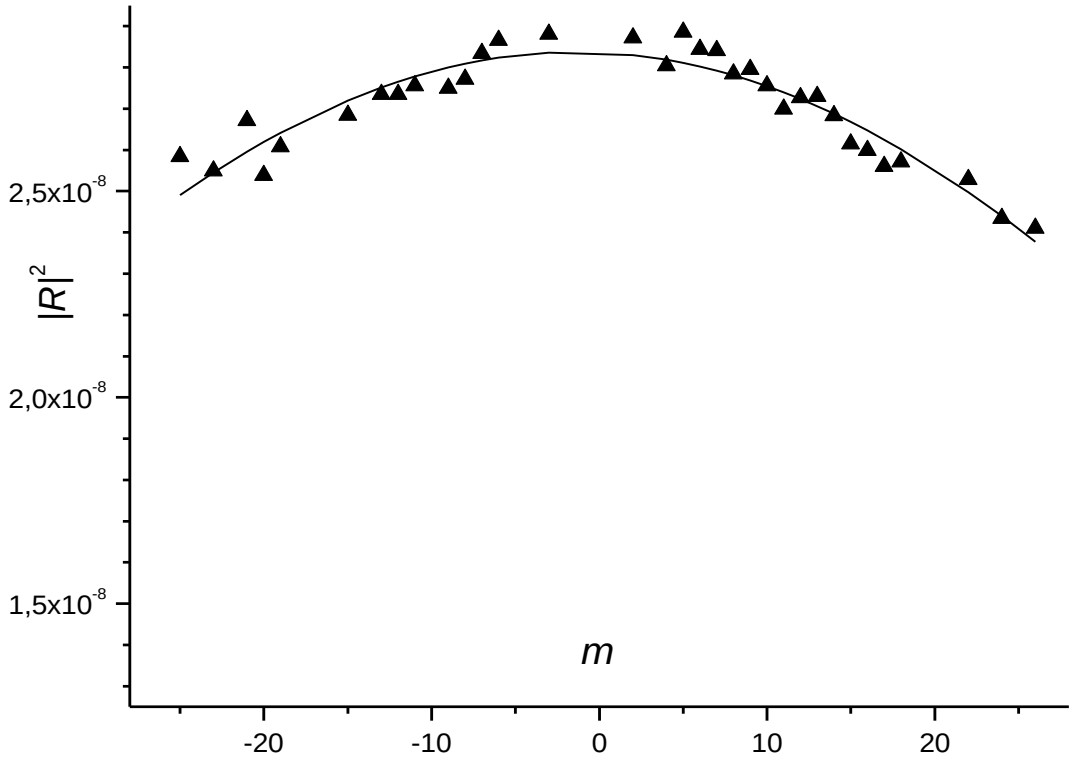

Fig. 1. Variation of the transition dipole moment squared $|R|^2$, in D^2 (1 D = 3.33546 × 10^{-30} C·m), vs. *m*, for the $\nu_1 + 2\nu_2 + (\nu_4 + \nu_5)^0_+$ band at 8556.60 cm^{-1}. The solid line represents the values calculated using the constants reported in Table 5. For this band, the rotational dependence is typical of what is usually observed for C_2H_2, and is well described by the Herman-Wallis factor, see Eq. (4).

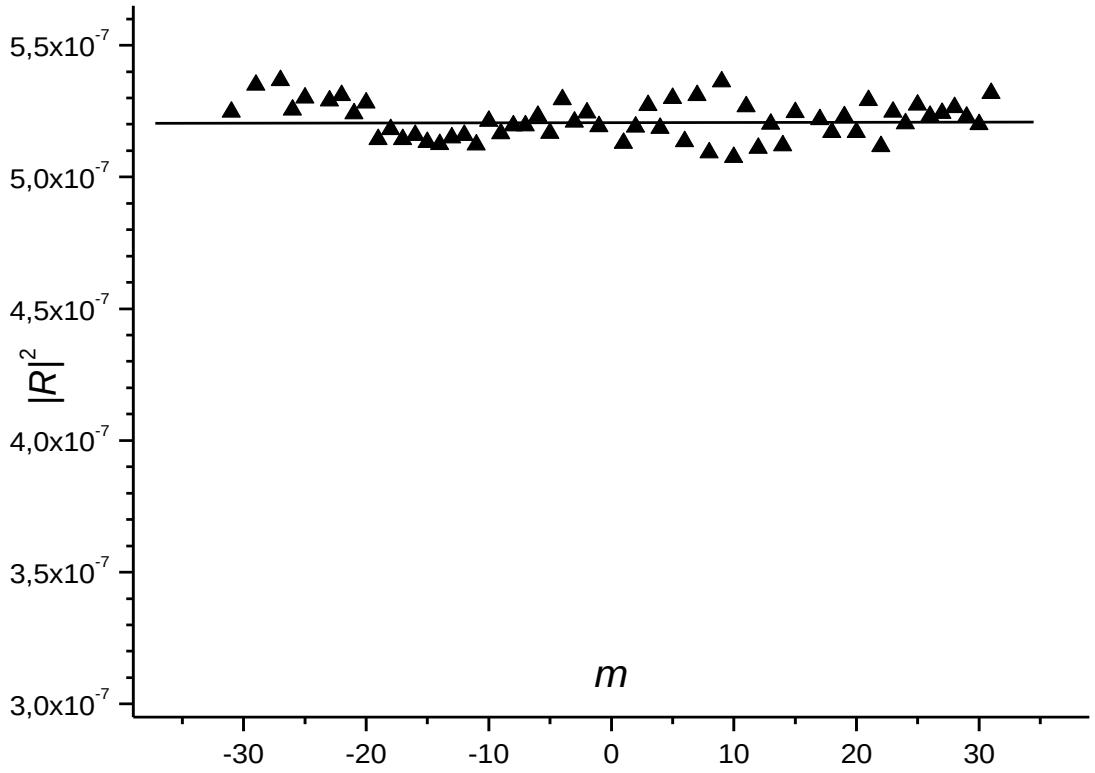

Fig. 2. Variation of the transition dipole moment squared $|R|^2$, in D^2 (1 D = 3.33546 × 10^{-30} C·m), vs. *m*, for the $\nu_1 + \nu_2 + \nu_3$ band at 8512.06 cm^{-1}. The horizontal line represents $|R_0|^2 = 5.21 \times 10^{-7}$ D^2 (see Tables 4 and 5). For this band, no rotational dependence is observed (the Herman-Wallis factor is equal to unity).

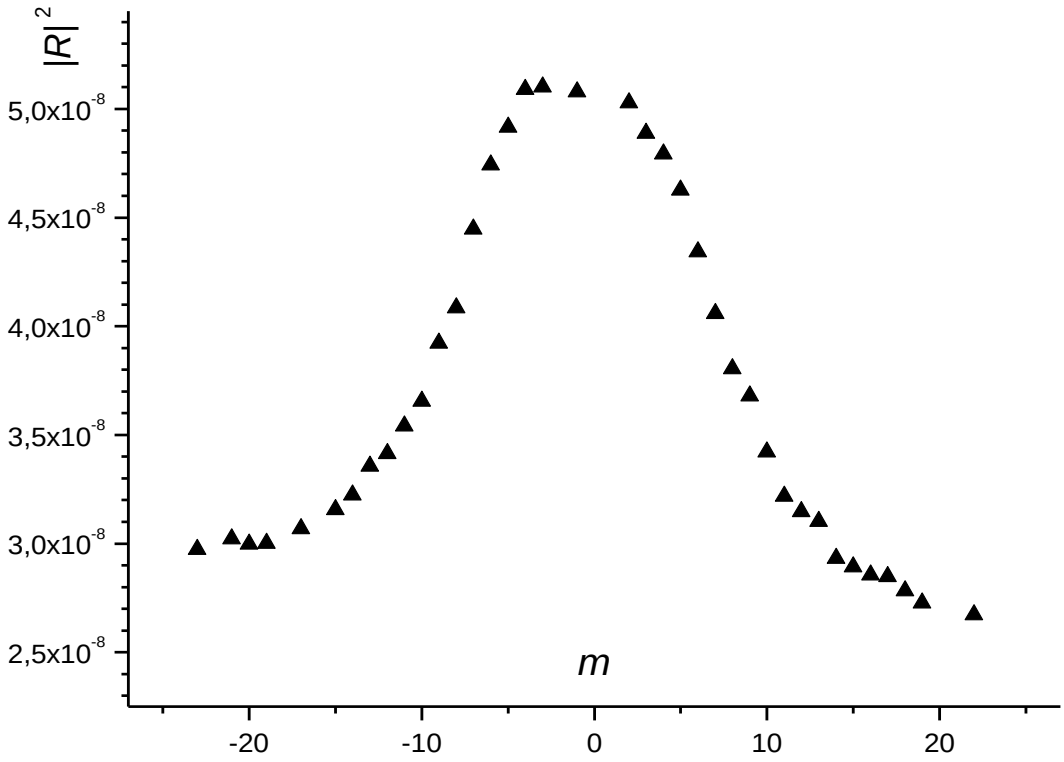

Fig. 3. Variation of the transition dipole moment squared $|R|^2$, in D^2 (1 D = 3.33546 × 10^{-30} C·m), vs. *m*, for the $\nu_1 + \nu_3 + 2\nu_4^0$ band at 7732.78 cm^{-1} (see Table 3). The Herman-Wallis factor is unadapted to fit such an unusual rotational dependence.